Nuclear Engineering and Technology 55 (2023) 902–907

Contents lists available at ScienceDirect

Nuclear Engineering and Technology

journal homepage: www.elsevier.com/locate/net

Original Article

Raman spectroscopy of eutectic melting between boride granule and stainless steel for sodium-cooled fast reactors

Hirofumi Fukai [a], Masahiro Furuya [b, *], Hidemasa Yamano [c]

[a] Waseda Research Institute for Science and Engineering, Waseda University, 3-4-1, Okubo, Shinjuku-ku, Tokyo, 169-8555, Japan
[b] Cooperative Major in Nuclear Energy, Graduate School of Advanced Science and Engineering, Waseda University, 3-4-1, Okubo, Shinjuku-ku, Tokyo, 169-8555, Japan
[c] Japan Atomic Energy Agency, 4002 Narita-cho, Oarai-machi, Higashiibaraki-gun, Ibaraki, 311-1393, Japan

ARTICLE INFO

Article history:
Received 12 July 2022
Received in revised form
15 November 2022
Accepted 16 November 2022
Available online 17 November 2022

Keywords:
Sodium-cooled fast reactor
Boron carbide
Stainless steel
Eutectic reaction
Raman spectroscopy

ABSTRACT

To understand the eutectic reaction mechanism and the relocation behavior of the core debris is indispensable for the safety assessment of core disruptive accidents (CDAs) in sodium-cooled fast reactors (SFRs). This paper addresses reaction products and their distribution of the eutectic melting/solidifying reaction of boron carbide (B_4C) and stainless-steel (SS). The influence of the existence of carbon on the B_4C-SS eutectic reaction was investigated by comparing the iron boride (FeB)-SS reaction by Raman spectroscopy with Multivariate Curve Resolution (MCR) analysis. The scanning electron microscopy with dispersive X-ray spectrometer was also used to investigate the elemental information of the pure metals such as Cr, Ni, and Fe. In the B_4C-SS samples, a new layer was formed between B_4C/SS interface, and the layer was confirmed that the formed layer corresponded to amorphous carbon (graphite) or FeB or Fe_2B. In contrast, a new layer was not clearly formed between FeB and SS interface in the FeB-SS samples. All samples observed the Cr-rich domain and Fe and Ni-rich domain after the reaction. These domains might be formed during the solidifying process.

1. Introduction

During a core disruptive accident (CDA) of sodium-cooled fast reactors (SFRs), dispersion of boron carbide (B_4C) in the core is a key to assessing accident progression [1]. The B_4C pellets are installed in the stainless steel (SS) cladding as a neutron absorber in SFRs. When the B_4C pellets contact SS, they melt in 1230 degrees Celsius or more due to the eutectic reaction, which is much lower than the melting temperature of B_4C (2500 degrees Celsius) and SS (1400 degrees Celsius) [2,3].

In the case of Fe-B system, the eutectic point is approximately 1200 degrees Celsius [4]. The eutectic point in the case of the Fe-B-C ternary system is almost equivalent to that in the case of Fe-B system [5,6]. When the CDA occurs on the SFRs, the control rod guide tubes are heated by the degraded core materials and melt. Then the cladding of the B_4C pellets melts by contact with the mixture of the molten SS and the degraded core materials. As a result, the B_4C pellets and the claddings melt by the eutectic reaction. The melt debris produced by the eutectic reaction might relocate widely in the core, which could enhance the neutron absorption of the disrupted core. Therefore, understanding the eutectic reaction mechanism and the relocation behavior of the core debris is indispensable for the safety assessment of CDAs in SFRs.

Japan Atomic Energy Agency and Japanese academic partners have been investigating physical properties and the eutectic reaction of B_4C and SS to implement their physical models to a severe accident computer code [7,8]. A visualization experiment of B_4C-SS eutectic reaction was carried out, and phase identification and morphological observation of reaction products [9], boron concentration in SS [7,9] and reaction kinetics of the eutectic reaction between B_4C and SS [10] were studied. And validation of a multiphase model for the eutectic reaction between molten SS and B_4C was extended to SIMMER IV [11].

To develop the physical models, it is indispensable to understand the eutectic reaction mechanism. In the past, several experimental studies on the eutectic reaction of B_4C-SS have been reported. Nagase et al. investigated the reaction kinetics of the eutectic reaction between B_4C and SS and defined the reaction rate

* Corresponding author.
E-mail addresses: furuya@aoni.waseda.jp (M. Furuya), yamano.hidemasa@jaea.go.jp (H. Yamano).

https://doi.org/10.1016/j.net.2022.11.010

constant of them from the reaction layer growth thickness or the decrease thickness of SS in the wide temperature range [2]. The overall reaction rate obeyed a parabolic raw and the reaction rate showed a discontinuity at the temperature between 1200 and 1225 degrees Celsius. These data were supported by other experimental data measured by differential thermal analysis (DTA) [12]. The microstructure and element distribution of the reaction products by Electron Probe Micro Analyzer (EPMA) and optical microscope have shown that the eutectic melt was initially formed on the SS side [13]. Sumita et al. reported in detail that the B_4C-SS melt infiltration into the SS grain boundaries was explained by grain boundary diffusion of boron [14–16]. In a place about the reaction product, the reaction products were not only metal-B-C compounds but also graphite [12,13]. It is expected that liquid phase carbon (graphite) exists during the eutectic reaction and the carbon might have affected the convection of the reacting products and the diffusion of boron. It is important to investigate the influence of carbon on the eutectic reaction.

This paper is intended to investigate B_4C-SS reaction products and their distribution after the eutectic melting/solidifying reaction process. The influence of the existence of carbon for the B_4C-SS eutectic reaction was investigated by comparing the FeB-SS reaction. Raman spectroscopy was applied to analyze the reaction products and their distribution. This instrument can analyze organic and inorganic materials in non-destruction and is superior in analyzing carbon in particular. Pshenichnikov et al. analyzed simulated debris of control blades by Raman spectroscopy and detected spectra of B_4C and carbon, and they showed the effectiveness of Raman spectroscopy [17]. In addition to these materials, the reaction products of a simple compound of Fe and B, which are distributed at the B_4C/SS interface region, were analyzed in this study. Elemental information on the eutectic melting of metals was also investigated with scanning electron microscopy (SEM) with an energy dispersive X-ray spectrometer (EDS).

2. Experimental

2.1. Eutectic reaction experiment

Table 1 shows the experimental conditions for eutectic reaction experiment. In SFRs, type 316L SS is used to cladding. For comparison of type 316L SS, this study also uses type 304 SS which was tested in the eutectic reaction experiment. As mentioned previously, FeB is also used for comparison to investigate the effect of the presence of carbon. The test specimen is the SS plates and boride (B_4C and FeB) granules. The SS plates are type 316L SS (Cr 16–18 %, Ni 10–14 %, Mn < 2 %, Si < 1 %, Mo 2–3 %, Fe Balance) and Type 304 SS (Cr 17–19 %, Ni 8–11 %, Mn < 2 %, Si < 1 %, Fe Balance) from Nilaco Co. The thickness of all plates was 0.3 mm. The plates were cut to size 3 mm in width and 3 mm in length approximately, and the specimens were washed with acetone, ethanol, and pure water to remove surface contamination.

Lump granules are B_4C (B > 76 %, C > 19.5 %, B2O3 < 0.5 %, Fe < 0.15 %, O < 1 %, N < 1 %, Si < 0.15 %) and FeB (99 %) from ESK Ceramics GmbH & Co. and Kojundo Chemical Lab. Co., Ltd, respectively. For the eutectic melting and solidifying experiment, the B_4C granules were crushed with a vise to make them smaller. Then, the SS plate was placed into an Al_2O_3 crucible (6 mm in inner diameter and 2.5 mm in depth), and the B_4C granule was placed on the plate. Finally, the crucible was placed on an Al_2O_3 boat, and the boat was loaded at the center of a tubular furnace, as shown in Fig. 1.

The tubular furnace has two sets of thermocouples. The tip of one set of thermocouples was attached to the outer wall of the Al_2O_3 tube for the furnace and is used for temperature control. The other is inserted in the Al_2O_3 tube and used to measure the temperature of the sample neighborhood. After being evacuated with a rotary pump and purged with argon gas (99.99995 vol.%), the sample was heated from room temperature (R.T.) to 1230–1245 degrees Celsius at a rate of 10 degrees Celsius per min and then was cooled to R.T. at a rate of 5 degrees Celsius/min under Ar gas flow (50 mL/min).

2.2. Temperature calibration

Fig. 2 shows the temperature curves of the tubular furnace's measured and preset temperatures of 1245 and 1230 degrees Celsius. The heating and cooling rate followed the programed temperature sufficiently at 800 degrees Celsius or higher measured temperature, which indicates the actual sample temperature, although the maximum measured temperature exceeded by 17 degrees Celsius set temperature. It is well known that the B_4C-SS eutectic melting temperature is approximately 1230 degrees Celsius, although the melting temperature of B_4C and SS are much higher. Therefore, eutectic melting occurs when the sample is heated up to 1230 degrees Celsius at a set temperature.

2.3. Raman spectroscopy analysis

After the eutectic melting and solidifying reaction, the samples were mounted in an epoxy resin and cut to the vertical direction, and then the cross-sections of the samples were polished to obtain a flat cross-section to analyze the reaction layer where the reaction products formed between B_4C and SS. These sample surfaces of the cross-section were analyzed by Raman spectroscopy (type NRS-5100 from Jasco Corp). A 5 mW, 532 nm green YAG laser was used as an excitation light source. Raman spectra of the cross-section surface were measured over 200 μm in width and 200 μm in length area with a 5 μm scanning interval. The Raman spectra are composed of the spectra of all reaction products in the laser spot area (4 μm in diameter), so the spectra were performed by Multivariate Curve Resolution (MCR) analysis in order to decompose to each spectrum [18,19].

2.4. SEM-EDS analysis

A Raman spectroscopy can analyze organic and inorganic materials and is superior in analyzing the carbon in particular. On the other hand, Raman spectroscopy cannot analyze pure metal. Therefore, the SEM (VE-7800, Keyence) with EDS (PV7750/75 ME,

Table 1
Experimental conditions for eutectic reaction experiment.

Boride granule	Type of the SS	Programed temperature of the tubular furnace (degrees celsius)
B_4C	316L	1245
B_4C	304	1245
FeB	316L	1230
FeB	304	1230

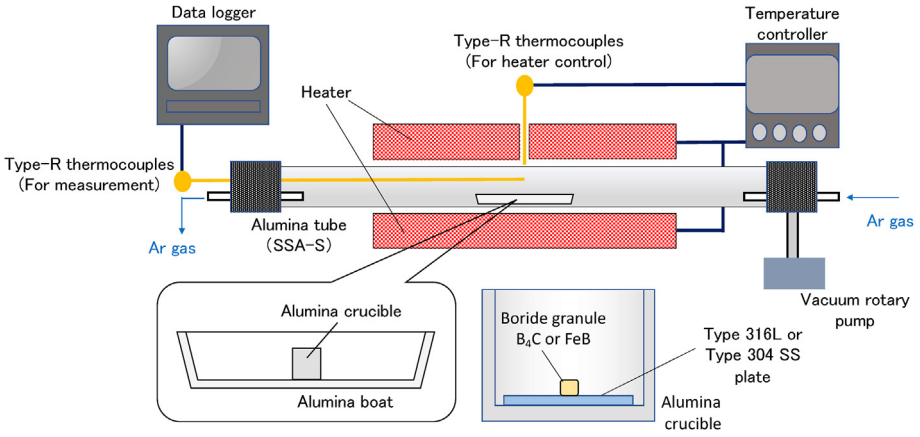

Fig. 1. An illustration of a tubular furnace for eutectic melting and solidifying reaction.

EDAX) was used to investigate elemental information such as Cr, Ni, and Fe. Elemental mapping images were obtained with an accelerating voltage of 20 kV for all elements. SEM-EDS's analysis area was almost the same as Raman spectroscopic analysis for each sample.

The detailed information of the element distribution after the eutectic melting and solidifying reaction is provided by making up for data of a Raman spectroscopy and data of SEM-EDS each other. These data are essential to measuring reaction products to understand the eutectic melting and solidifying reaction.

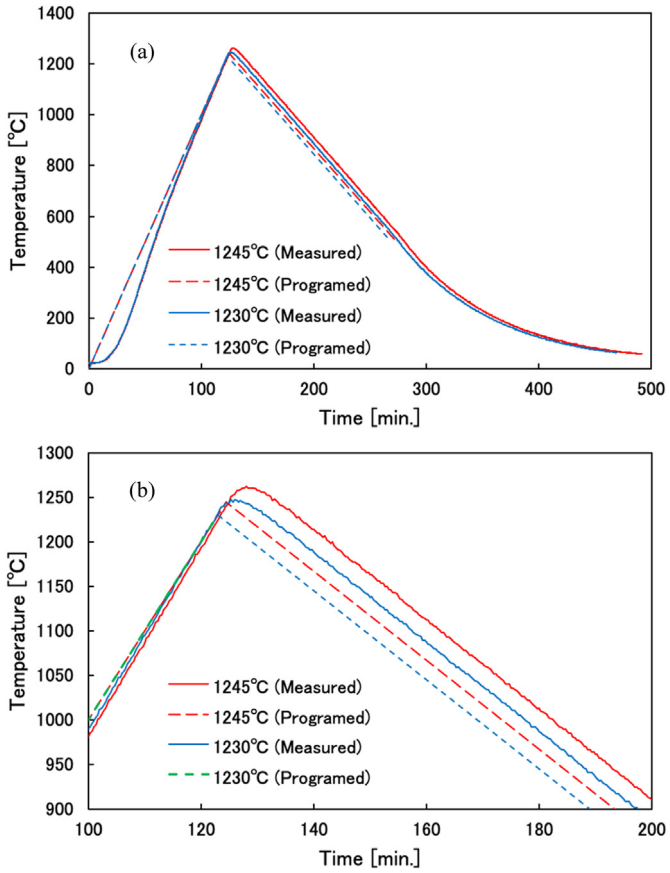

Fig. 2. (a) Temperature curves of the tubular furnace's measured and programed temperature of 1245 and 1230 degrees Celsius, (b) Enlarged view.

3. Results and discussion

3.1. Raman spectroscopy with MCR method

Fig. 3 shows the top view before and after the eutectic melting and solidifying reaction and cross-section, which across the granule sample remained after the reaction, after each sample's eutectic melting and solidifying reaction. The areas surrounding the yellow square are indicated for the Raman spectroscopy analysis performed later. In all samples, the eutectic melting between the boride granule and SS progressed approximately concentrically towards the outside from the point at which B_4C or FeB granule was placed, and the granule slightly remained as unreacted. Notably, FeB-SS samples reacted at a slightly low temperature in the case of B_4C-SS samples.

After the eutectic melting and solidifying reaction, the cross-section of the samples was analyzed by Raman spectroscopy to

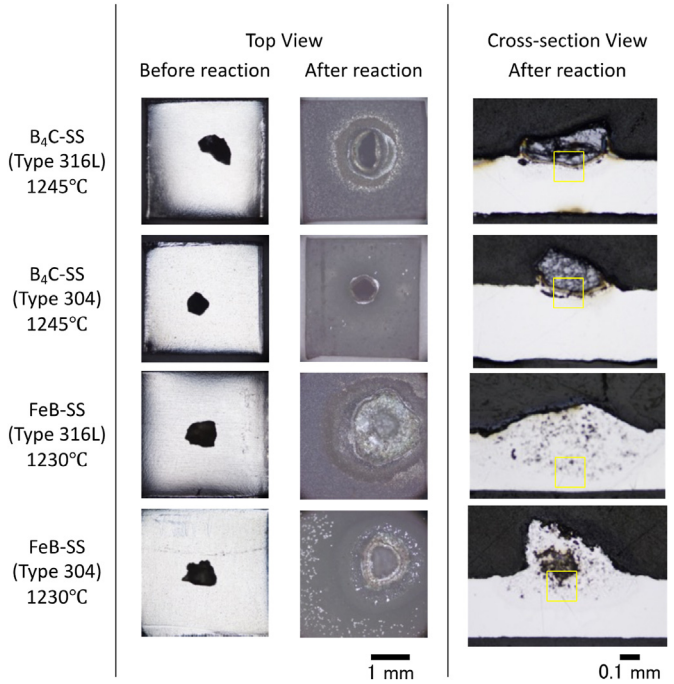

Fig. 3. Top view photos before and after the eutectic melting /solidifying reaction and cross-section photos after each sample's eutectic melting and solidifying reaction.

investigate elemental information. Fig. 4 shows the elemental maps by Raman spectroscopy with MCR analysis and microscope images around the analyzed area. The yellow square areas indicate the area of Raman spectroscopy analysis.

In the B_4C-SS samples, a new layer was formed between B_4C and SS interface. This result was consistent with that by Shibata et al. [20]. Two to four layers were observed at the interface when it was enlarged more, and the chemical composition was different at each point in each layer. The present study confirmed that the formed layer corresponded to amorphous carbon (graphite) or FeB or Fe_2B from the Raman spectrum retrieved by MCR analysis, as shown in Fig. 5. It is difficult to separate these because the spectrum of these compounds are similar each other. The layer might be formed as a mixture of these compounds from the comparison with another report [21]. According to more detailed reports, the layer consists of graphite, γ-Fe, FeB, Fe_2B, and more complex boride for instant $Fe_3(C, B)$, $(Cr, Fe)_2B$, $(Cr, Fe)_{23}(C, B)_6$ [6,22]. These reports suggest the same compounds in our experiment with Raman spectroscopy, although Raman spectroscopy cannot identify the complex boride because Raman spectroscopy has fewer databases than other analysis methods such as X-ray diffraction.

In the B_4C-SS samples, a new thin layer was formed between B_4C and SS interface as wrote earlier. In contrast, a new layer was not clearly formed between FeB and SS interface, but the same spectrum of amorphous carbon or FeB or Fe_2B has also obtained in FeB-Type 304 SS samples around the FeB granule. Unfortunately, no Raman spectra were obtained in FeB-Type 316L SS samples. The reason will be discussed later. As the Raman spectrum of carbon was not detected from SUS304 before the eutectic reaction experiment, there is no carbon element in FeB-Type 304 SS eutectic reaction system; thus, the spectrum corresponded to FeB or Fe_2B, which might be un-reacted FeB and a part reacted FeB (maybe Fe_2B).

There is an intriguing difference between the B_4C-SS reaction and the FeB-SS reaction. In the B_4C-SS samples, a layer was clearly formed between the B_4C and SS interface consisting of graphite and borides. There is the clear difference between the B_4C-SS reaction and the FeB-SS reaction whether there is carbon in reaction system although the influence on the reaction system of the carbon is still unknown. We investigated influence on reaction system of the carbon in detail with a future problem.

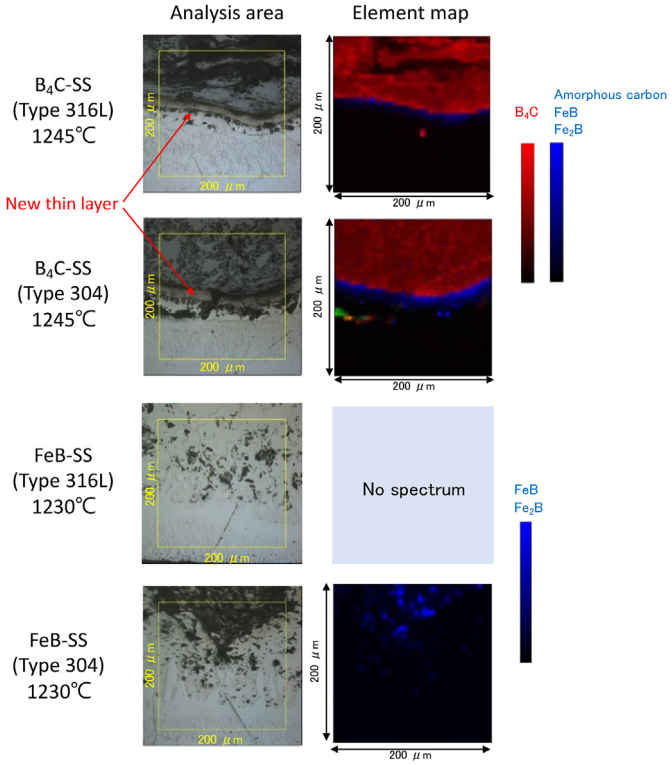

Fig. 4. Elemental maps by Raman spectroscopy with MCR analysis.

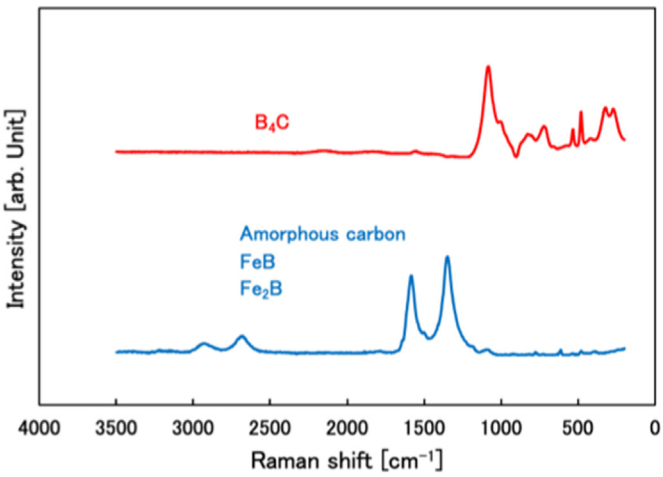

Fig. 5. Raman spectra of B_4C (red line) and amorphous carbon (graphite) or FeB or Fe_2B (blue line) retrieved by MCR analysis (in the case of B_4C-SS(Type 316L), 1245°C). (For interpretation of the references to color in this figure legend, the reader is referred to the Web version of this article.)

3.2. Elemental distribution analysis by SEM-EDS

Because Raman spectroscopy cannot analyze pure metals, no information was obtained from the lower half part of the analyzed area of Raman spectroscopy in Fig. 4. Therefore, the SEM with EDS was also used to investigate the elemental information of the pure metals such as Cr, Ni, and Fe. Fig. 6 shows SEM images and EDS element maps. SEM-EDS's analyzed area was almost the same area of Raman spectroscopy in each sample. Elemental distribution of Cr, Ni, and Fe was observed in the analysis area where no spectrum was obtained for Raman spectroscopic analysis. A deflection was observed in the distribution of Cr from the EDS element maps. The eutectic melting and solidifying reaction region is divided into approximately two domains: the Cr-rich domain and Fe and Ni-rich domain, and the distribution of the domains corresponding to a distribution of light and shade of SEM images. These domains might be formed during solidifying reactions because the shape of the domains' boundary was roundish and intricate. These characteristics are addressed in the reports [22]. No significant Raman shift peak was found in FeB-Type 316L SS samples since the area was covered with Cr and Ni-rich layer, which diffused from Type 316L SS as shown in Fig. 6.

There was no difference between the interface layers of B_4C and SS regardless of the type of SS. The main difference between Type 316L SS and Type 304 SS is the density of Cr and Ni, although it was not significant. It indicates that such differences in Cr and Ni density do not affect the eutectic reaction between borides and SS. However, it has been reported that Mo, which slightly exists only in Type 316L SS, affected the eutectic reaction [22]. There was no influence on the eutectic reaction of Mo in the present study. It will be necessary to perform a more detailed analysis and confirm the effect of Mo and other small amounts of elements.

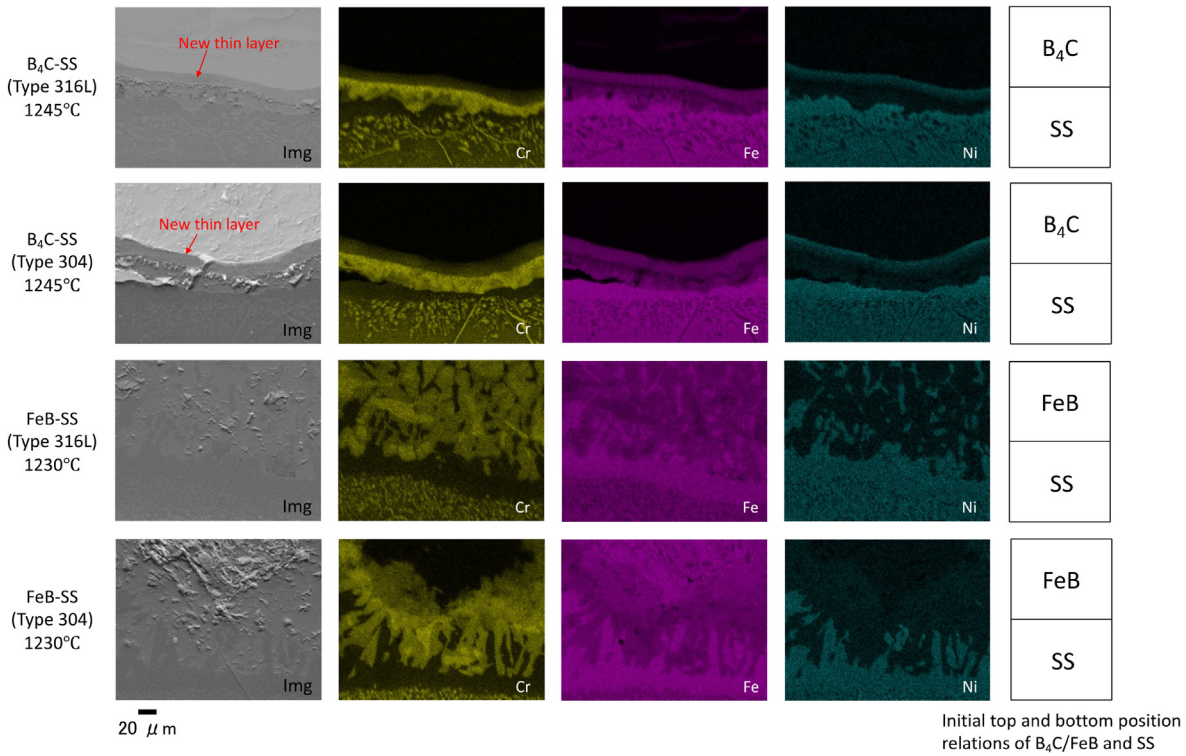

Fig. 6. SEM images and EDS element maps.

4. Conclusion

In this study, the eutectic melting samples of boride (B_4C and FeB) and SS (Type 316L and Type 304) were investigated using Raman spectroscopy on the basis of MCR analysis. SEM-EDS was also used to investigate the elemental information of the pure metals such as Cr, Ni, and Fe. After the eutectic melting of the B_4C-SS samples, a new layer was clearly formed at the interface B_4C and SS layers, and it was confirmed that the formed layer corresponded to amorphous carbon (graphite), FeB, or Fe_2B. Moreover, the Cr-rich domain and Fe and Ni-rich domain were also observed in all samples. These results were consistent with that of previous reports. In contrast, a new layer was not clearly formed between FeB and SS interface in the FeB-SS samples. As the main difference between the B_4C-SS reaction and the FeB-SS reaction was existing carbon or not., the influence on reaction system of the carbon will be investigated with a future problem. In addition, the influence of chromium boride on the convection of the reacting products during the eutectic reaction will be also investigated.

Declaration of competing interest

The authors declare that they have no known competing financial interests or personal relationships that could have appeared to influence the work reported in this paper.

Acknowledgments

This work was supported by the "Technical development program on a fast reactor common basis" entrusted to the Japan Atomic Energy Agency (JAEA) by the Ministry of Economy, Trade and Industry (METI).

References

[1] T. Takai, T. Furukawa, H. Yamano, Thermophysical properties of austenitic stainless steel containing boron carbide in a solid state, Mechanical Engineering Journal 8 (2021), 20-00540.
[2] F. Nagase, H. Uetsuka, T. Otomo, Chemical interactions between B4C and stainless steel at high temperatures, Journal of Nuclear Materials 245 (1997) 52–59.
[3] M. Takano, T. Nishi, N. Shirasu, Characterization of solidified melt among materials of UO2 fuel and B4C control blade, J. Nucl. Sci. Technol. 51 (2014) 859–875.
[4] T.B. Massalski, Binary Alloy Phase Diagram, ASM International, Ohio, 1990, p. 482.
[5] A. Sudo, T. Nishi, N. Shirasu, M. Takano, M. Kurata, Fundamental experiments on phase stabilities of Fe-B-C tarnary systems, J. Nucl. Sci. Tech. 52 (2015) 1308–1312.
[6] J. Lentz, A. Röttger, W. Theisen, Solidification and phase formation of alloys in the hypoeutectic region of Fe-C-B system, Acta Materialia 99 (2015) 119–129.
[7] H. Yamano, T. Takai, T. Furukawa, S. Kikuchi, Y. Emura, K. Kamiyama, H. Fukuyama, H. Higashi, T. Nishi, H. Ohta, X. Liu, K. Morita, K. Nakamura, Study on eutectic melting behavior of control rod materials in core disruptive accidents of sodium-cooled fast reactors: (1) Project overview and progress until, in: The 2020 International Conference on Nuclear Engineering (ICONE2020), Online, 2018, V002T08A007.
[8] H. Yamano, T. Takai, T. Furukawa, S. Kikuchi, Y. Emura, K. Kamiyama, H. Fukuyama, H. Higashi, T. Nishi, H. Ohta, K. Morita, K. Nakamura, Study on eutectic melting behavior of control rod materials in core disruptive accidents of sodium-cooled fast reactors: (1) Project overview and progress until, in: The 2021 International Conference on Nuclear Engineering (ICONE28), Online, 2019, V003T12A008.
[9] H. Yamano, T. Takai, T. Furukawa, Post-test material analysis of eutectic melting reaction of boron carbide and stainless steel, Transactions of the Japan Society of Mechanical Engineers 86 (2020), 19-00360.
[10] S. Kikuchi, T. Takai, H. Yamano, K. Sakamoto, Study on eutectic melting behavior of control rod materials in core disruptive accidents of sodium-cooled fast reactors: (2) Kinetic study on eutectic reaction process between stainless with low boron carbide concentration and stainless steel, in The 2021 International Conference on Nuclear Engineering (ICONE28), Online, V003T12A003.
[11] X. Liu, K. Morita, H. Yamano, Study on eutectic melting behavior of control rod materials in core disruptive accidents of sodium-cooled fast reactors: (4) Validation of a multi-phase model for eutectic reaction between stainless steel and boron carbide, in The 2020 International Conference on Nuclear Engineering (ICONE2020), Online, V002T08A019.

[12] S. Kikuchi, H. Yamano, K. Nakamura, Study on eutectic melting behavior of control rod materials in core disruptive accidents of sodium-cooled fast reactors: (3) Kinetic study of boron carbide-stainless steel eutectic melting by differential thermal analysis, in The 2020 International Conference on Nuclear Engineering (ICONE2020), Online, V002T08A004.
[13] S. Kikuchi, K. Nakamura, H. Yamano, Kinetic study on eutectic reaction between boron carbide and stainless steel by differential thermal analysis, Mechanical Engineering Journal 8 (2021), 20-00542.
[14] T. Sumita, K. Urata, Y. Morita, Y. Kobayashi, Dissolution behavior of core structure materials by molten corium in boiling water reactor plants during severe accidents, Journal of Nuclear Science and Technology 55 (2018) 267–275.
[15] T. Sumita, Y. Kobayashi, Investigation of corrosion-erosion behavior of stainless steel considering SS-B4C melt, Journal of Nuclear Materials 515 (2019) 71–79.
[16] T. Sumita, Y. Kobayashi, Dissolution behavior of solid stainless steel by its molten eutectic mixture with B4C under dynamic condition, Progress in Nuclear Energy 117 (2019), 103094.
[17] A. Pshenichnikov, Y. Nagae, M. Kurata, Raman characterization of the simulated control blade debris to understand the boric compounds transformations during severe accidents, Mechanical Engineering Journal 7 (2020), 19-00477.
[18] M. Ando, H. Hamaguchi, Molecular component distribution imaging of living cells by multivariate curve resolution analysis of space-resolved Raman spectra, Journal of Biomedical Optics 19 (2014), 011016, 2014.
[19] S. Elumalai, S. Manago, A.C.D. Luca, Raman microscopy: progress in research on cancer cell sensing, Sensors 20 (2020) 5525.
[20] H. Shibata, K. Sakamoto, A. Ouchi, M. Kurata, Chemical interaction between granular B4C and 304L-type stainless steel materials used in BWRs in Japan, Journal of Nuclear Science and Technology 52 (2015) 1313–1317.
[21] M. Aizenshtein, I. Mizrahi, N. Froumin, S. Hayun, M.P. Dariel, N. Frage, Interface reaction in the B4C/(Fe-B-C) system, Materials Science and Engineering A 495 (2008) 70–74.
[22] T. Sumita, T. Kitagaki, M. Takano, A. Ikeda-Ohno, Solidification and re-melting mechanisms of SUS-B4C eutectic mixture, Journal of Nuclear Materials 543 (2021), 152527.